PERGAMON

International Journal of Solids and Structures 37 (2000) 6683–6704

INTERNATIONAL JOURNAL OF SOLIDS and STRUCTURES

www.elsevier.com/locate/ijsolstr

Formation of a shear localization in structural elements under transverse dynamic loads

Q.M. Li [1], Norman Jones*

Impact Research Centre, Department of Engineering, University of Liverpool, Brownlow Street, Liverpool, L69 3GH, UK

Received 27 October 1998; received in revised form 11 May 1999

Abstract

The formation of a transverse shear localization (shear hinge) in a beam element made from a ductile material and subjected to transverse dynamic loads is studied in the present paper. Dimensional analysis and a finite-element simulation are used to describe the formation and structure of a transverse shear hinge. It is shown that the beam response under a transverse dynamic load is determined by two dimensionless parameters, represented by the relative values of loading velocity and loading time. When the actual impact or impulsive loading velocity is of the same order as the characteristic loading velocity, then the concept of a shear hinge is relevant. In this case, a quasi-static method of an analysis can be used to obtain the length of a shear hinge, and the shear strain within the shear hinge may be determined from the shear sliding displacement obtained using a rigid, perfectly plastic analysis. Other response modes and strain rate effects are also discussed. It transpires that the current conclusions are also applicable to circular plates and cylindrical shells.

Keywords: Shear localization; Dynamic loading; Dynamic response of structural elements

1. Introduction

It is well-known that transverse shear becomes an increasingly important factor in the dynamic response and failure of transversely loaded structural elements as the dynamic loading rate and intensity increases (Symonds, 1968; Jones, 1989a, b, c; Jones and Shen, 1993). The concept of a 'shear hinge (or shear sliding)' was employed in these studies to investigate the first stage of the response in those

* Corresponding author. Tel.: +44-151-794-4858; fax: +44-151-794-4848.
E-mail address: njones@mechnet.liv.ac.uk (N. Jones).
[1] Current address: Division of Structures and Mechanics, School of Civil and Structural Engineering, Nanyang Technological University, Nanyang Avenue, Singapore 639798.

0020-7683/00/$ - see front matter
PII: S0020-7683(99)00162-6

Nomenclature

c^2	N_0L^2/M_0R
c_p	transverse plastic shear wave speed given by Eq. (1)
e	half length of a plastic shear hinge
f	yield function
m	M/M_0
n	N/N_0
q	Q/Q_0
s_{ij}	deviatoric stress components defined by Eq. (15)
t	time
w, W	transverse displacements
x	spatial coordinate
B	beam width
D, p	coefficients in Cowper–Symonds relationship in Eq. (23)
E_h	linear hardening modulus in a uniaxial tensile test
E_t	linear hardening modulus in a pure shear test
H	beam thickness
L	half length of beam or cylindrical shell
M, Q, N	bending moment, transverse shear force and circumferential membrane force (in cylindrical shell)
M_0, Q_0, N_0	fully plastic bending moment, transverse shear force and circumferential membrane force capacities of a cross-section
R	radius of a circular plate
T	loading time
T^*	e/c_p, characteristic response time
V	velocity
γ	transverse engineering shear strain
ε_e, $\dot{\varepsilon}_e$	equivalent strain and strain rate
η_v, η_t	dimensionless parameters defined in Eqs. (25a and b)
ν	$Q_0L/2M_0$ for beam and cylindrical shell, or $Q_0R/2M_0$ for circular plate, also used as Poisson's ratio when declared
ξ	x/L
ρ	material density
σ_0	uniaxial tensile yield stress
σ_e	von-Mises equivalent stress
τ	transverse shear stress

structural elements for which transverse shear deformation dominates the bending and membrane deformations. Usually, it is assumed that a shear hinge has an infinitesimal length for a rigid, perfectly plastic idealisation. This assumption emerges from Symonds' (1968) conclusion that a transverse shear hinge is always stationary in a rigid, perfectly plastic beam, which implies that transverse shear will be localized within the initially formed zone when the influence of material strain hardening is neglected. Symonds' conclusion, which was based on a particular square yield surface, has been extended to arbitrary regular and singular yield conditions, and has been shown by Li (2000) to be valid for symmetrically loaded circular plates and cylindrical shells.

No attempt was made to explore the structure of a shear hinge in Symonds' (1968) original work and the subsequent studies on structural elements. These studies concentrated mainly on global structural responses, where the concept of shear and bending hinges can give a reasonable prediction of the energy consumed without knowing the exact dimensions of shear and bending hinges, and the actual deformation process within them. In fact, shear and bending hinges are infinitesimally long in dynamic plastic analyses using a rigid, perfectly plastic material. The energy consumed within a plastic hinge may be estimated from the relative transverse displacement across the shear hinge, or the relative rotation angle across a bending hinge, respectively. However, if the results from rigid, perfectly plastic analyses are used to predict the initiation of local failures or local flow instabilities, then an estimation of the sizes of shear and bending hinges are required in order to obtain the deformation details within these hinges.

Usually, combined bending and shearing responses develop first in a structural element under transverse dynamic loads (Jones, 1985, 1989a). This is followed by a combined bending and membrane response and, finally, membrane behaviour dominates if no material failure has occurred during the response. However, one of several failure modes might initiate at any stage during the response, as observed by Menkes and Opat (1973) for beams, which have been studied theoretically by Jones (1976, 1989c). The present investigation focuses on the early time response period when shearing and bending effects dominate and sometimes lead to a transverse shear failure or adiabatic shear instability depending on the loading rate and material properties. A study of the transition between these two different shear failures has been presented by Li and Jones (1999).

A transverse shear localization might develop at the site of the impact loading and at hard point support interfaces, and is formed by the propagation of the transverse disturbance away from these interfaces. The propagation of transverse disturbances in one or two-dimensional structural elements, such as beams, plates and shells, is complicated due to the existence of free surfaces on the top and bottom surfaces of a structural element. However, for low loading rates, the inertia or wave propagation effect may be neglected. In this case, the formation of a shear localization might be treated as a quasi-static problem, as studied by Wen et al. (1995a) and Wen and Jones (1996) for a beam and a circular plate, respectively. These methods will be re-examined in section 2 of the present paper with a more solid physical basis and will be extended to cylindrical shells. Several investigations have used the simplification of a quasi-static behaviour to determine the size of a shear hinge in order to study material failure, and observed encouraging results when compared with experimental results (Wen et al., 1995a–c; Jones et al., 1997).

When the loading rate and intensity are high, material failure might occur while the transverse disturbance is still propagating across a structure. The actual strain and strain rate cannot be determined from the shear hinge length predicted by a quasi-static analysis and wave propagation theory is necessary to provide a realistic prediction. Wang and Jones (1996) proposed a transverse shear propagation model within the scope of rigid-plastic analyses when retaining the influence of material strain hardening. It was found that the transverse shear disturbance will propagate with a constant velocity

$$c_{\mathrm{p}} = \sqrt{\frac{E_{\mathrm{t}}}{\rho}}, \tag{1}$$

where E_{t} is the linear hardening modulus in a pure shear test and ρ is the material density. Clearly, the influence of the top and bottom free surfaces of structural elements on the propagation of the transverse shear disturbance are neglected, which is, nevertheless, important for the actual shear wave propagation in a beam, as shown in section 3. A possible relationship between the quasi-static method and a wave

propagation analysis is studied numerically in section 3 from this view-point, and, thus, a description of transverse shear localization in structural elements is presented, which might be used in material failure and flow instability analyses.

2. Quasi-static analyses

2.1. Introduction

A shear dominant zone may develop in a beam section when subjected to a pair of opposite displacements at two sides of the section,

$$W(x = L) = -W(x = -L) \tag{2}$$

as shown in Fig. 1 for the quasi-static case. A necessary condition for the appearance of such a shear dominant zone is that the length of the beam section is sufficiently short. It is expected that a shear dominant deformation mode will become a bending dominant deformation mode with an increase of the beam section length. The critical value of this length for the transition between these two deformation modes defines the shear hinge length in a quasi-static analysis, which will be studied in sections 2.3–2.5 for beams, plates and cylindrical shells, respectively.

The beam problem in Fig. 1 can be idealized as a static plane strain problem, and the validity of the above postulate is examined by using the finite-element code ABAQUS. Four node bi-linear plane strain elements are used for an aluminum-alloy 6061-T6 beam. The material is modelled by an elastic-plastic model with a uniaxial tensile yield stress $\sigma_0 = 286.8$ MPa and strain hardening modulus $E_h = 542.6$ MPa. Two typical results from the ABAQUS analyses are presented in Fig. 2(a) and (b) for two different values of L/H, where L and H are the half length and the thickness of a beam section, respectively. It is evident that the deformation mode corresponding to a large value of L/H is a bending dominant deformation mode (Fig. 2 (a)) and the one corresponding to a small value of L/H is a shear dominant deformation mode (Fig. 2(b)). Therefore, it is assumed that there exists a transition point from a shearing dominant mode to a bending dominant mode with an increase of L/H. This transition condition is used to estimate the shear hinge length in a beam.

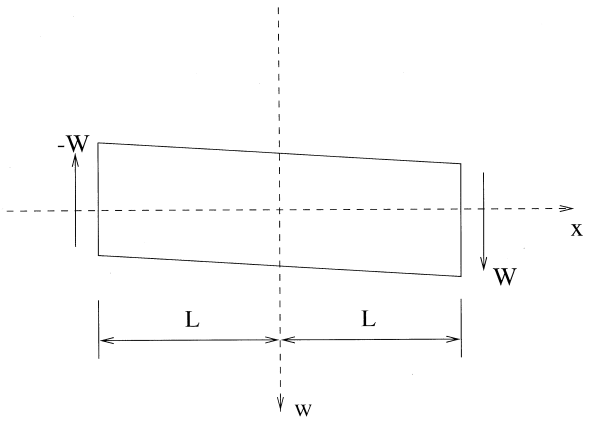

Fig. 1. Boundary condition for the beam problem.

2.2. Basic equations

A generalized yield condition is described by

$$f(q, m, \ldots) = 0 \tag{3}$$

where, $q = Q/Q_0$ and $m = M/M_0$, when Q_0, and M_0 are the static fully plastic transverse shear force and bending moment capacities of the cross-section, respectively. The normality rule of plasticity requires

$$\mathrm{d}\gamma = \mathrm{d}\lambda \frac{\partial f}{\partial q} \quad \text{and} \quad \mathrm{d}\kappa = \mathrm{d}\lambda \frac{\partial f}{\partial m}, \tag{4a,b}$$

where $\mathrm{d}\gamma$ and $\mathrm{d}\kappa$ are the increments of transverse shear strain and bending curvature, respectively. Eq. (4a,b) are associated with the transverse shear force and bending moment through the energy dissipation relations. Therefore, the generalized stresses on a yield surface satisfy the following requirements

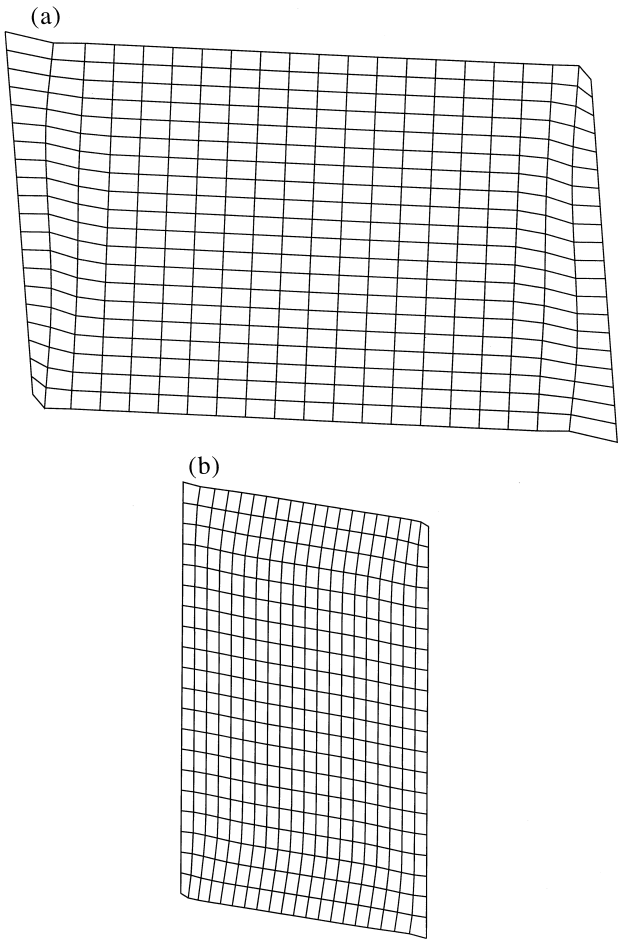

Fig. 2. Static simulation of the plane strain problem in Fig. 1 for 6061-T6 aluminum alloy in Table 1 without considering strain rate effect, (a) bending mode, $L/H = 0.8$; (b) shearing mode, $L/H = 0.3$, where $H = 9.52$ mm.

$$\left|\frac{\partial f}{\partial m}\right| \gg \left|\frac{\partial f}{\partial q}\right| \geq 0 \tag{5a}$$

for a bending dominant hinge and

$$\left|\frac{\partial f}{\partial q}\right| \gg \left|\frac{\partial f}{\partial m}\right| \geq 0 \tag{5b}$$

for a shear dominant hinge.

For many yield conditions relating q and m, Eqs. (5a) and (5b) would require

$$\|m\| \approx 1 \tag{6a}$$

for a bending dominant hinge and

$$\|q\| \approx 1 \tag{6b}$$

for a shear dominated hinge.

In particular, an independent yield condition between q and m, i.e. $|q| = 1$ and $|m| \leq 1$, or $|m| = 1$ and $|q| \leq 1$, described as a square in q-m plane (Gomes de Oliveira and Jones, 1978; Li and Jones, 1995a), is used to simplify the following analyses and to provide an estimate for a shear dominant hinge length. In this case, Fig. 2 (a) and (b) are two possible responses according to Eq. (2) associated with Eqs. (6a) and (6b), respectively. The maximum length for the occurrence of a shear dominant deformation is now determined using a quasi-static method of analysis for three different structural elements.

2.3. Beam

The static equilibrium equations for a beam may be written in the form (Li and Jones, 1995a)

$$\frac{\partial Q}{\partial x} = 0 \tag{7a}$$

and

$$Q + \frac{\partial M}{\partial x} = 0. \tag{7b}$$

If a shear mode is initiated in a beam then Eqs. (5b) and (6b) must be satisfied within the length of a shear dominant zone (shear hinge), $\Delta = 2e$. Eqs. (6b) and (7a) require $|Q| \approx Q_0$ within the shear hinge, so that integrating Eq. (7b) from $x = -e$ to $x = e$ gives

$$e = -\frac{M(x = e) - M(x = -e)}{2Q_0}. \tag{8}$$

The maximum value of e is determined when the bending mode is just initiated at the two ends ($x = \pm e$), i.e. $M(x = e) = -M(x = -e) = -M_0$, which terminate the further extension of shear deformations, and, thus, define the length of a shear hinge,

$$e = \frac{M_0}{Q_0} = \frac{\sqrt{3}}{4}H = 0.433H \tag{9}$$

for a beam with a solid rectangular cross-section. A similar method was used by Wen et al. (1995a), in

which $M(x = e) = 0$ was assumed giving a value of e which is one-half of the present value, i.e. $e = 0.216H$. An ABAQUS simulation of the idealized shear dominant zone in Fig. 2 (b) has shown that a shear dominant behaviour will occur at $L = 0.3H$. The value of e for a circular plate in section 3.2 is $0.325-0.342H$, approximately, which is larger than Wen et al.'s (1995a) value for a beam, but smaller than the value given by Eq. (9). Because there are more restraints in a circular plate than in a beam, the value of e for a circular plate should be smaller than the value for a beam according to physical intuition. This evidence supports the present prediction, but further verification is necessary.

2.4. Circular plate

The static equilibrium equations for a circular plate are (Li and Jones, 1994)

$$\frac{\mathrm{d}(Qr)}{\mathrm{d}r} = 0 \quad \text{and} \quad \frac{\mathrm{d}M_{\mathrm{r}}}{\mathrm{d}r} + \frac{M_{\mathrm{r}} - M_{\theta}}{r} + Q = 0. \tag{10a,b}$$

Eq. (10a) gives $Qr = -Q_0 a$ if $Q = -Q_0$ is first reached at $r = a$. Therefore, $Q(r = a + \Delta r) = -Q_0/(1 + \Delta r/a)$, where $\Delta r/a \leq e/a$ and $e/a \sim H/a \ll 1$ is required in order to satisfy the plate assumptions. For example, a may be the radius of a circular plate for a uniform impulsive pressure loading, or the radius of a blunt projectile for a mass impact problem. Thus, $Q \approx -Q_0$ within the shear hinge.

Under the further assumption that $M_{\mathrm{r}} = M_{\theta}$ in the immediate vicinity of the shear hinge, a static analysis has been presented by Wen and Jones (1996) to give a shear hinge length

$$e = \frac{1 + \sqrt{3}}{8} H = 0.342H, \tag{11}$$

where the von-Mises yield condition was used to relate M_{r} and M_{θ}. If the Tresca yield condition is used instead, then a similar procedure gives the shear hinge length

$$e = \frac{3\sqrt{3}}{16} H = 0.325H. \tag{12}$$

2.5. Cylindrical shell

The static equilibrium equations for a cylindrical shell are (Li and Jones, 1995b)

$$\frac{\mathrm{d}M}{\mathrm{d}x} + Q = 0 \quad \text{and} \quad \frac{\mathrm{d}Q}{\mathrm{d}x} - \frac{N}{R} = 0, \tag{13a,b}$$

which may be written in the dimensionless forms

$$\frac{\mathrm{d}m}{\mathrm{d}\xi} = -2\nu q \quad \text{and} \quad \frac{\mathrm{d}q}{\mathrm{d}\xi} = \frac{c^2 n}{\nu}, \tag{14a,b}$$

where $m = M/M_0$, $n = N/N_0$, $q = Q/Q_0$, $\xi = x/L$, $\nu = Q_0 L/2M_0$ and $c^2 = N_0 \mathrm{L}^2/M_0 R$.

An independent yield condition relating m, q and n is assumed here. It is evident that a circumferential strain is always associated with a transverse shear flow, while strains associated with bending are expected to remain small in a shear hinge. Thus, material yielding only leads to significant circumferential and shear deformations in a shear hinge. Therefore, an interactive yield condition between transverse shear and the circumferential membrane force in a shear hinge is sufficient for

predicting the distributions of shear force within a shear hinge, although the existence of a bending moment is important for satisfying the equilibrium Eq. (14a).

The stress state in a shear hinge, which may enter the interactive yield condition between q and n, is characterised by $\sigma_{33}=\sigma_\theta$ and $\sigma_{12}=\tau$. Now, the von-Mises equivalent stress is

$$\sigma_e = \sqrt{\frac{3}{2}s_{ij}s_{ij}}, \tag{15}$$

where

$$s_{ij} = \sigma_{ij} - \left(\frac{1}{3}\sigma_{kl}\delta_{kl}\right)\delta_{ij},$$

which leads to (p. 344 in Jones, 1989a)

$$\sigma_\theta^2 + 3\tau^2 = \sigma_0^2 \tag{16}$$

or

$$n^2 + q^2 = 1 \tag{17}$$

when using $\sigma_0 = \tau_0\sqrt{3}$, $N=\sigma_\theta H$ and $Q=\tau H$.

Substituting Eq. (17) into Eq. (14b) gives the dimensionless shear force

$$q = \cos\left(\frac{c^2}{v}\xi\right) \tag{18}$$

when using $q = 1$ at $\xi=0$. Eqs. (14a) and (18) with the boundary conditions $m=-1$ at $\xi=e/L$ and $m = 1$ at $\xi=-e/L$ predict

$$\sin\left(2\sqrt{3}\frac{e}{R}\right) = \frac{3}{2}\frac{H}{R}. \tag{19}$$

Now, $e/R \ll 1$ for a cylindrical shell problem, which gives $\sin(2e\sqrt{3}/R)\approx 2e\sqrt{3}/R$, so that, Eq. (19) simplifies to

$$e \approx \frac{\sqrt{3}}{4}H \approx 0.433H \tag{20}$$

which is identical to the shear hinge length of a beam in Eq. (9).

2.6. Remarks

Experimental studies on the dynamic behaviour of beams have shown that the main region of a transverse shear hinge consists of an anti-symmetrical simple shear flow. A good example of a typical shear dominant zone is shown in Fig. 12 of Zener (1948). Similar results can also be found in Jones (1989c) although considerable bending deformations are evident on both sides of the shear hinge. These anti-symmetrical features of an idealised transverse shear hinge in the dynamic case are similar to the idealised quasi-static problem in Fig. 1. However, when bending and membrane deformations are introduced, the problem becomes more complicated, which will not be discussed in the present paper.

It is evident that the response of a beam under transverse quasi-static and dynamic loads is very

Table 1
Material properties of 6061-T6 aluminum alloy (E, E_h, p and D: ABAQUS (1996b); ν: J. Appl. Phys., 72, 429–441 (1992); ρ, σ_0: Jones (1976))

E (GPa)	ρ (kg/m^3)	σ_0 (MPa)	ν	E_h (MPa)	p	D (1/s)
72.4	2686	286.8	0.32	542.6	4.0	6500.0

different. In the static case, the bending deformation mode usually dominates over the shear deformation mode when there are no hard-point restraints near to the loading point[1], because the low loading rate ensures that bending deformations absorb plastic strain energy rather than the shear deformation mode. However, with a rapidly increasing loading intensity in the dynamic case, the condition for initiating shear deformation may be satisfied first at the loading location, which starts to absorb plastic strain energy and leads to the subsequent propagation of a transverse shear disturbance into the beam. The shear deformation will be confined within a limited distance because bending, and then membrane, deformations will prevent the further propagation of the shear disturbance. Thus, the determination of a shear hinge length in the dynamic case is the same as for the quasi-static method introduced in sections 2.1–2.5 when strain rate and inertia effects are neglected, which are, nevertheless, examined numerically in the following sections. However, this observation does not prevent the retention of strain rate and inertia effects in the equilibrium and constitutive equations when studying the global responses of these structural elements.

3. Propagation of a transverse shear deformation in a beam

3.1. Description of the problem

The material properties and beam dimensions for the test results reported in Menkes and Opat (1973) are used in the following discussion.

The simplification of a rigid, perfectly plastic material leads to stationary transverse plastic shearing according to Symonds (1968). However, when material strain hardening is considered, the transverse shear disturbance will propagate along a structural element at a constant propagation velocity for a linear strain hardening beam, as shown by Wang and Jones (1996). This is a first order approximation since reflections of a plane shear wave from the upper and lower free surfaces of a beam are neglected. Even within the characteristic length of a localized transverse shear zone (shear hinge), wave scattering is important. In order to understand the propagation of a transverse disturbance in a beam, an idealized problem described below is studied using a finite-element simulation.

Any wave effects through the thickness of a structural element are neglected in the following analysis. It has been shown that a shear hinge has an anti-symmetrical pattern. Thus, the transverse shear disturbance is applied at the anti-symmetrical plane, and only one-half of the shear hinge is studied. The transverse displacement, $W(t)$, is described by

[1] The hard-point restraints may cause the initiation of the shear deformation mode because of a short distance between a pair of the external opposite forces.

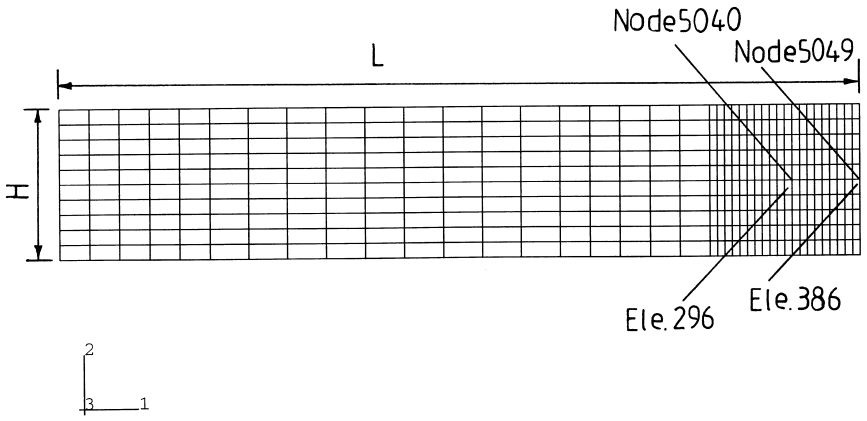

Fig. 3. Plane strain finite element of a beam.

$$W(t) = W\frac{t}{T}, \quad \text{for} \quad 0 \le t \le T \quad \text{and} \quad W(t) = W \quad \text{for} \quad t > T, \tag{21}$$

in which T can be adjusted to represent different loading rates. The beam material is elastic–plastic with a linear strain hardening relationship

$$\sigma_e = \sigma_0 + E_h \varepsilon_e, \tag{22}$$

where σ_0 and E_h are the uniaxial tensile yield stress and the hardening modulus given in Table 1. The influence of material strain rate sensitivity may be included through the Cowper–Symonds relationship (Jones, 1989a)

$$\dot{\varepsilon}_e = D\left(\frac{\sigma_e}{\sigma_e^s} - 1\right)^p, \tag{23}$$

where $\dot{\varepsilon}_e$ is the equivalent plastic strain rate, σ_e^s is the equivalent static stress, σ_e is the equivalent stress at a non-zero plastic strain rate and D and p are constants given in Table 1.

Plane strain four-node bi-linear elements (CPE4) in ABAQUS/standard-5.5 are used in the simulation, as shown in Fig. 3. Direct implicit time integration is used in the dynamic analysis in ABAQUS/standard and an automatic time step control based on the half-step residual concept is selected in the simulation. Newton's method was employed for solving the nonlinear equilibrium equations using the Hilber–Hughes–Taylor operator with an artificial damping parameter $\alpha = -0.05$ and Newmark's formula were used for the displacement and velocity integration. For more details of the numerical procedure, the reader may refer to the ABAQUS Theory and User's Manuals, Version 5.5 (1996a).

3.2. Dimensional analysis

A complete group of independent dimensionless variables for the prescribed model are

$$\frac{B}{H}, \frac{L}{H}, \nu, p, TD, \frac{V}{c_e}, \frac{V}{c_p}, \frac{\sigma_0}{E}, \frac{W}{H}, \tag{24a–i}$$

where $e = 0.433H$ is one half of the shear hinge length given by Eq. (9). $V = W/T$ is the driving velocity

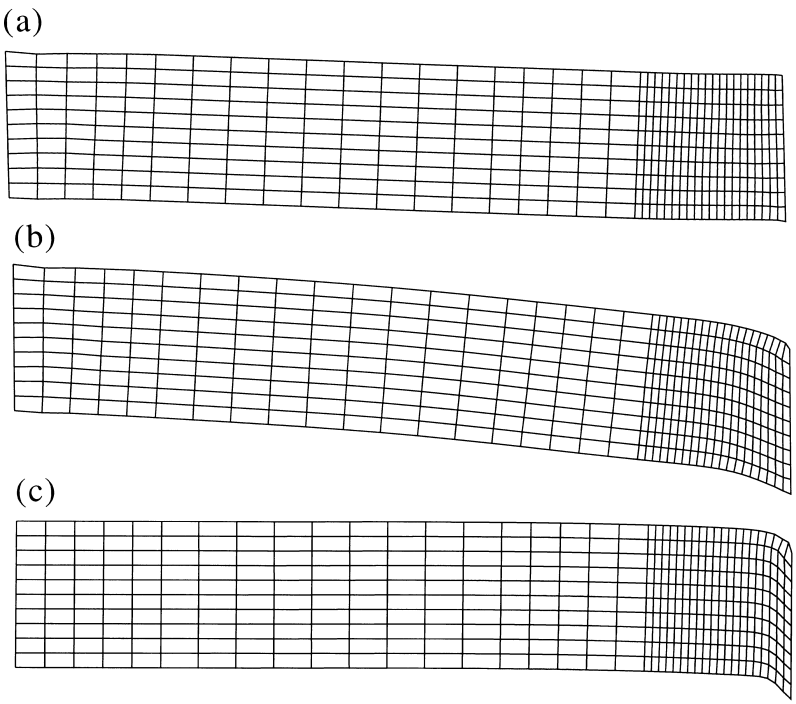

Fig. 4. Response mode of a transversely loaded beam, (a) bending dominant deformation mode (H4); (b) shear hinge deformation mode (H6); (c) shear wave propagation mode (H1).

at one end of the beam. $c_e = \sqrt{(E/2(1+\nu)\rho)}$ and $c_p = \sqrt{(E_h/3\rho)}$ are the elastic and plastic shear wave speeds[2], respectively. In the following analyses, further postulates are introduced, i.e.

1. Material strain rate effects are neglected. Thus, p and TD can be eliminated from the group.
2. The present beam problem may be treated as a plane strain problem because $2.67 \leq B/H \leq 5.36$ for the beams tested by Menkes and Opat (1973). Therefore, B/H and ν are eliminated from the group.
3. The beam response is dominated by large plastic deformations, i.e. elastic effects are neglected in the analyses. Thus, σ_0/E and V/c_e are removed from the dimensionless groups.
4. L/H is an important factor in the transverse shear response (Jones, 1989a), which is reflected in the parameter $\nu = Q_0 L/(2M_0) = 2L/H$ which governs the initiation of the transverse shear response mode in a beam with a rectangular cross-section. However, it is likely that the size of the transverse shear localization zone does not depend on this parameter if $L/H \gg 1$.
5. The external work is determined by W/H, which may influence the characteristics of a shear localization. When the driving velocity is a constant, the dimensionless time $T/(e/c_p)$ may be introduced to represent the external work, equivalently, instead of W/H.

Thus, only two dimensionless parameters are significant for describing a shear localization zone, i.e.

[2] According to the von-Mises yield condition, the linear hardening modulus in a pure shear test is given by $E_t = E_h/2(1+\nu) = E_h/3$ when the material is incompressible ($\nu = 0.5$), where E_h is determined from a uniaxial tensile test.

Table 2
Numerical simulation data (H = 9.52 mm, B = 25.4 mm, L = 101.6 mm). Note: (a): bending mode ($\eta_v \ll 1$); (b): trapped shear hinge ($\eta_v < 1$ and $\eta_v \sim o(1)$), in which (b1) and (b2) correspond to $\eta_t < 1$ and $\eta_t > 1$, respectively; (c): transient shear wave propagation ($\eta_v > 1$), in which (c1) and (c2) correspond to $\eta_t < 1$ and $\eta_t > 1$, respectively

No.	W (mm)	T (μs)	V (m/s)	η_v	η_t	Type	Note
H1	1.5	5	300	1.154	0.32	(c1)	
H2	6.5	500	13	0.05	31.55	(a)	
H3	3.0	50	60	0.23	3.16	(b2)	
H4	5.0	150	33.33	0.13	9.46	(a)	
H5	3.0	10	300	1.154	0.63	(c1)	
H6	3.0	20	150	0.58	1.26	(b2)	
H7	1.5	10	150	0.58	0.63	(b1)	
H8	3.0	20	150	0.58	1.26	(b2)	strain rate
H9	3.0	10	300	1.154	0.63	(c1)	
H10	6.0	20	300	1.154	1.26	(c2)	Fig. 11 (c)
H11	6.0	40	150	0.58	2.52	(b2)	
H12	9.0	60	150	0.58	3.79	(b2)	
H13	9.0	30	300	1.154	1.89	(c2)	Fig. 11(d)

$$\eta_v = \frac{V}{c_p} \quad \text{and} \quad \eta_t = \frac{T}{e/c_p}, \tag{25a,b}$$

where $c_p = 260$ m/s and $T^* = e/c_p = 15.85$ μs are the respective characteristic velocity and response time of the particular beam with H = 9.52 mm studied by Menkes and Opat (1973).

The finite-element simulations show that three cases are possible, i.e. (a) $\eta_v \ll 1$, or $V \ll c_p$; (b) $\eta_v \sim o(1)$, or $V \sim o(c_p)$; (c) $\eta_v > 1$, or $V > c_p$. These three cases correspond to a static or quasi-static process, a dynamic plastic response process and a transient wave propagation process, respectively, as shown in Figs. 4(a)–(c). However, two different situations in both case (b) and case (c) are distinguished when η_t

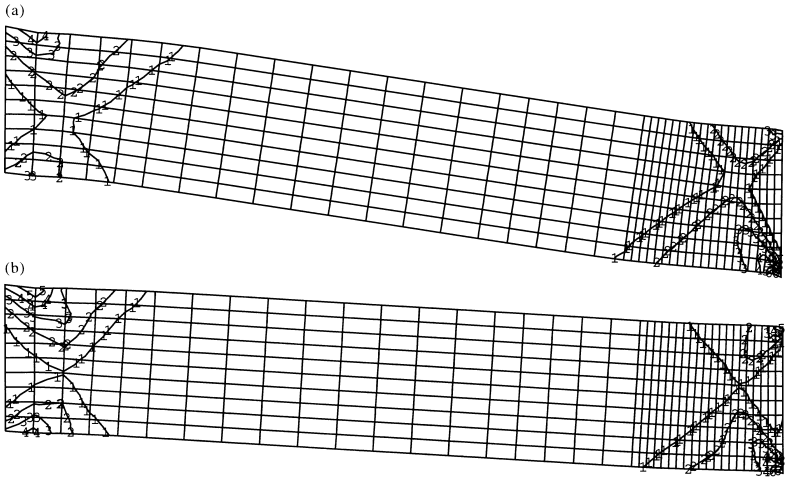

Fig. 5. Distributions of equivalent plastic strain in bending responses, (a) W = 6.5 mm and T = 500 μs (H2), the equivalent plastic strain values are (1) 0.02, (2) 0.06, (3) 0.10, (4) 0.14, (5) 0.18, and (6) 0.22; (b) W = 5 mm and T = 150 μs (H4), the equivalent plastic strain values are (1) 0.02, (2) 0.044, (3) 0.069, (4) 0.093, (5) 0.12, and (6) 0.14.

≤ 1 (see (b1) and (c1) in Table 2) and $\eta_t > 1$ (see (b2) and (c2) in Table 2), which will be discussed in a subsequent section.

3.3. Finite-element simulations

The three different cases (a)–(c) in section 3.2 are simulated by the examples in Table 2 with several loading rates and impact velocities.

3.3.1. Bending response when $V \ll c_p$

Two simulations are conducted with $V \ll c_p = 260$ m/s. The parameters $T = 500$ μs and $W = 6.5$ mm are used for the first example, which gives $V = 13$ m/s and $V/c_p = 0.05$. A second example with $T = 150$ μs and $W = 5.0$ mm gives $V = 33.3$ m/s and $V/c_p = 0.128$. The final distributions of the equivalent plastic strains for these two examples are shown in Fig. 5 (a) and (b), respectively. It is evident that both beams have a typical bending response, as shown previously in Fig. 2(a) and 4(a). Thus, the response mode when $V \ll c_p$ is a bending dominant deformation.

The non-symmetrical distributions of the equivalent strains about the mid-plane of the beam are due

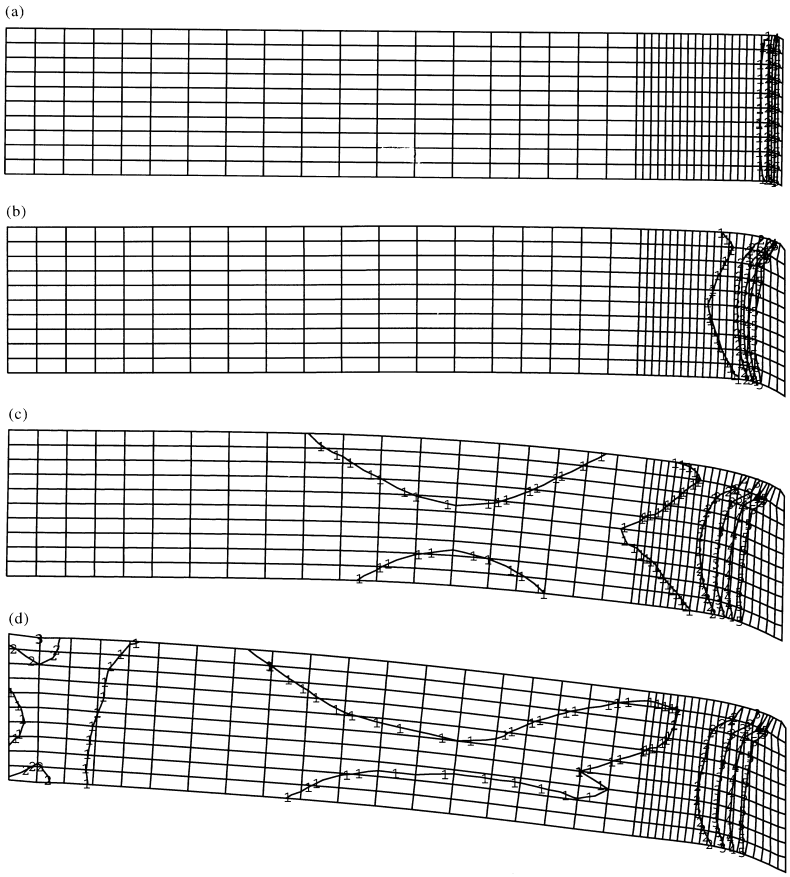

Fig. 6. Propagation of equivalent plastic strain for $W = 3.0$ mm and $T = 20$ μs (H6), the equivalent plastic strain values are (1) 0.01, (2) 0.058, (3) 0.11, (4) 0.15, and (5) 0.20, (a) at $t = 2.18$ μs, (b) at $t = 10.47$ μs, (c) at $t = 25.00$ μs, and (d) at $t = 70.00$ μs.

to the influence of the membrane force because the two ends of the beam are restrained in the horizontal direction.

3.3.2. Plastic shear hinge formation when $V \sim o(c_p)$

The propagation of equivalent plastic strains, which consists mainly of the transverse shear component of the strain tensor, are shown in Fig. 6 for $T = 20$ μs and $W = 3.0$ mm with $V = 150$ m/s, or $V/c_p = 0.58$. It is observed that there is a localised transverse shear zone near the loaded end. This shear deformation is propagated at 240 m/s, approximately, up to a time of $T^* = 15.85$ μs according to the first three simulation results in Fig. 6. This speed is approaching the plastic shear wave speed, $c_p = 260$ m/s, and, therefore, the propagation model proposed by Wang and Jones (1996) is adequate. However, for times $T > T^*$, the propagated shear deformations are trapped in a zone having a length, $e \approx 0.433H$, as determined by the quasi-static analysis in section 2.3. Stress distributions in the beam are complicated due to the reflections of stress waves on the upper and lower free surfaces and the clamped ends. The propagation of the axial stress obtained by the ABAQUS simulation indicates the formation of a bending mode at about one-third of the beam length from the impacted end of the beam, which is probably responsible for preventing any further propagation of the shear deformation. Thus, stress wave interactions are important for the formation of plastic shear and bending hinges. Similar observations were made by Reid and Gui (1987) who used ABAQUS with beam elements to study the propagation of a plastic bending hinge in a Parkes' cantilever beam. It was found that the effect of the reflection of an elastic bending wave may lead to a 'hinge arrest mechanism', which locks the plastic hinge at about one-half of the cantilever beam span for a short period. The response characteristics of the beam studied by Reid and Gui (1987) are different from the present problem because shear and axial deformations, which are important here, are not significant in Parkes' problem. However, it is evident that stress wave interactions have an important influence on the formation of a plastic hinge. The stress wave effects were examined by Yu and Jones (1989, 1997) for fully clamped beams subjected to a mass impact. The interactions between wave dispersion and reflection lead to peak values of the bending moments, and result in significant plastic bending deformation regions, which explains the initial formation of the plastic hinges. Yu et al. (1997) also examined the interaction between a plastic bending hinge and elastic flexural wave in a cantilever beam.

Many authors have estimated the transverse shear strain by assuming a uniform strain distribution within a transverse shear hinge. In order to verify the validity of this assumption, Fig. 7 (a) gives the plastic shear strain histories at different locations along the length of a shear hinge where curves 1–9 correspond to the plastic shear strains in elements 296, 306, ... 366 and 376 on the mid-plane shown in Fig. 3. The size of each element is $H/20$ so that the ten elements cover the length $0.5H$ which is larger than one-half the length of a shear hinge ($0.433H$) according to the quasi-static analysis in section 2.3. The shear hinge is completely established after around 16 μs according to Fig. 7(b). This is similar to the time that a plastic shear wave travels one-half the length of a shear hinge, i.e. $0.43H/c_p$. The shear strain distribution in the shear hinge is not uniform and consists of a main shear zone with nearly constant shear strain in the centre of the shear hinge and a transition zone with decreasing shear strains towards the end of the show hinge, as shown in Figs. 6 and 7(a).

It is interesting to examine the validity of the traditional method for calculating the transverse shear strain in a shear hinge, i.e.

$$\gamma = \frac{\Delta W}{e}, \tag{26}$$

where γ is the engineering shear strain and W is the relative transverse displacement across the shear hinge (e) between nodes 5049 and 5040 in Fig. 3. The calculations by ABAQUS in Fig. 7(b) give $\Delta W =$

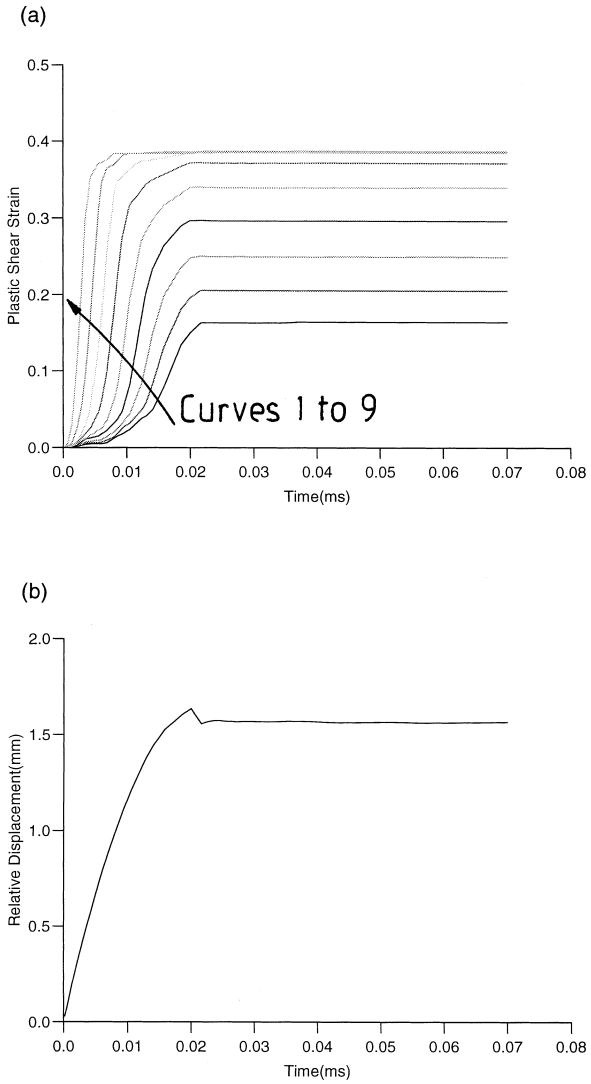

Fig. 7. (a) Plastic shear strain histories at different locations along the shear hinge length in simulation H6, curves 1, 2, ... 9 correspond to elements 296, 306, ... 376 shown in Fig. 3; (b) relative displacement across the shear hinge length, e.

1.55 (mm), so that Eq. (26) gives $\gamma = 1.55/(0.433 \times 9.52) = 0.38$. From Fig. 7(a), the maximum engineering shear strain (ABAQUS always uses the engineering value) is about 0.39[3]. Thus, γ in Eq. (26) provides a good estimate of the maximum engineering plastic strain in a shear hinge. A similar conclusion is obtained from another simulation example, H3 in Table 2, with $V/c_p = 0.231$. The calculated relative transverse displacement across the shear hinge is 0.447 mm, which gives $\gamma = 0.447/(0.433 \times 9.52) = 0.11$ from Eq. (26), and is very close to the calculated value $\gamma_{max} = 0.103$ from ABAQUS.

[3] Normally, the shear strain in the element near to the boundary (element 386) is not accurate due to the influence of the boundary on the strain calculation. Therefore, the connecting element (element 376) is used to estimate the maximum shear strain.

When the loading time is smaller than the characteristic time, $T^* = e/c_p = 15.85$ μs, the transverse shear deformation can only propagate a short distance before the loading ceases. This distance is smaller than the shear hinge length obtained from a quasi-static method of analysis. Fig. 8(a)–(d) demonstrate four different cases with the same impact velocity $V = 150$ m/s corresponding to (a) $W = 1.5$ mm and $T = 10$ μs, (b) $W = 3.0$ mm and $T = 20$ μs, (c) $W = 6.0$ mm and $T = 40$ μs and (d) $W = 9.0$ mm and $T = 60$ μs. It is evident that the length of the localised shear zone in Fig. 8(a) is smaller than the predicted shear hinge length, e. The relative transverse displacement across the shear hinge is $\Delta W \approx 1.20$ mm, which gives $\gamma \approx 1.20/(0.433 \times 9.52) = 0.29$ according to Eq. (26). This value is smaller than $\gamma_{max} = 0.38$ from the ABAQUS simulation results. Therefore, plastic shear wave propagation effects must be considered for $T < T^*$ even when $V < c_p$.

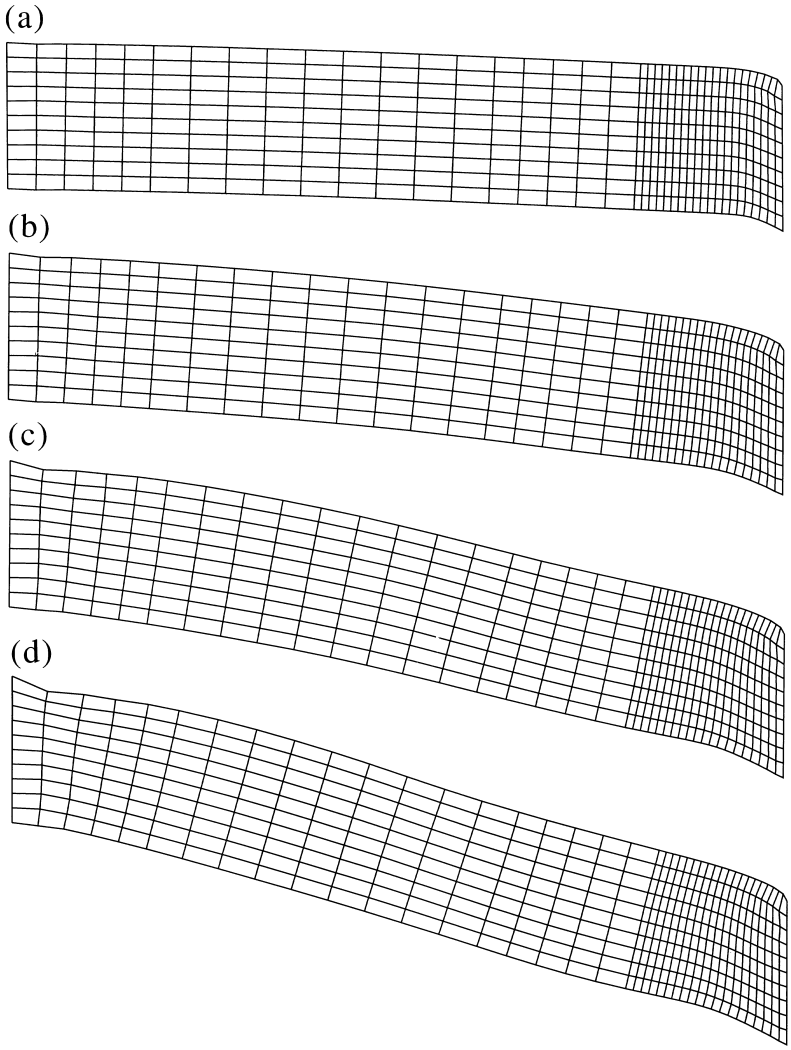

Fig. 8. Deformation patterns of a beam with an imposed velocity of $V = 150$ m/s, (a) $W = 1.5$ mm and $T = 10$ μs (H7); (b) $W = 3.0$ mm and $T = 20$ μs (H6); (c) $W = 6.0$ mm and $T = 40$ μs (H11); (d) $W = 9.0$ mm and $T = 60$ μs (H12).

The maximum plastic shear strains for the simulations in Fig. 8(a)–(d) have an almost constant value of 0.38, which implies that the maximum shear strain is determined mainly by the magnitude of the impact velocity for a given beam.

3.3.3. Shear propagation when $V > c_p$

For the loading parameters $T = 5$ μs and $W = 1.5$ mm, which give $V = 300$ m/s and $V/c_p = 1.15$, Figs. 9 and 10 present results similar to Figs. 6 and 7. One important difference is that the transverse shear deformations localize into a narrow zone which is smaller than the calculated shear hinge length $e = 0.433H$. When the loading time T is smaller than $T^* = e/c_p$, the transverse shear deformations cannot reach the distance, e, determined by a quasi-static method of analysis, before the energy input ceases, as shown in Fig. 11(a) and (b). In this case, a quasi-static analysis cannot be used to predict a realistic shear hinge length. Instead, wave propagation of the transverse shear disturbance must be considered as suggested by Wang and Jones (1996). According to Fig. 10(b) and Eq. (26), the maximum shear strain in the shear hinge length ($e = 0.433H$) is 0.39, which is much smaller than the numerical calculated maximum value of $\gamma_{max} = 0.83$ in Fig. 10(a) obtained using the ABAQUS simulations.

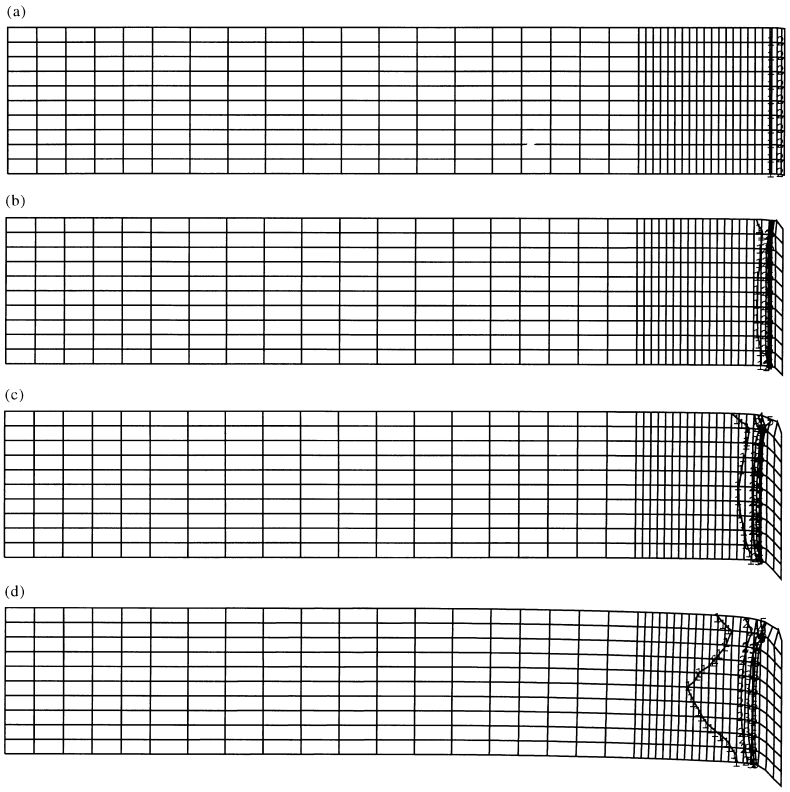

Fig. 9. Propagation of equivalent plastic strain for $W = 1.5$ mm and $T = 5$ μs with $V = 300$ m/s (H1), the equivalent plastic strain values are (1) 0.01, (2) 0.058, (3) 0.11, (4) 0.15, and (5) 0.20, (a) at $t = 0.22$ μs, (b) at $t = 2.20$ μs, (c) at $t = 4.61$ μs, and (d) at $t = 10.00$ μs.

When the loading time is longer than $T^* = e/c_p$, the shear deformations are not trapped within the calculated shear hinge length and a large shear zone is observed, as shown in Fig. 11(c) and (d). The propagation of shear deformations cannot be predicted by a shear wave theory for $T > T^*$ because a bending mode is involved outside the shear domain region. However, this situation develops rarely in practice because material failure occurs normally for high impact velocities, which prevents the input of any more external impact energy for $T > T^*$. Again, the maximum shear strains are similar for different loading parameters but having the same imposed velocity, where γ_{max} are 0.833, 0.844, 0.844 and 0.850 for H6, H9, H10 and H13 in Table 2, respectively. This confirms the observation made in section 3.3.2 that the imposed velocity is an important factor for determining the maximum shear strain.

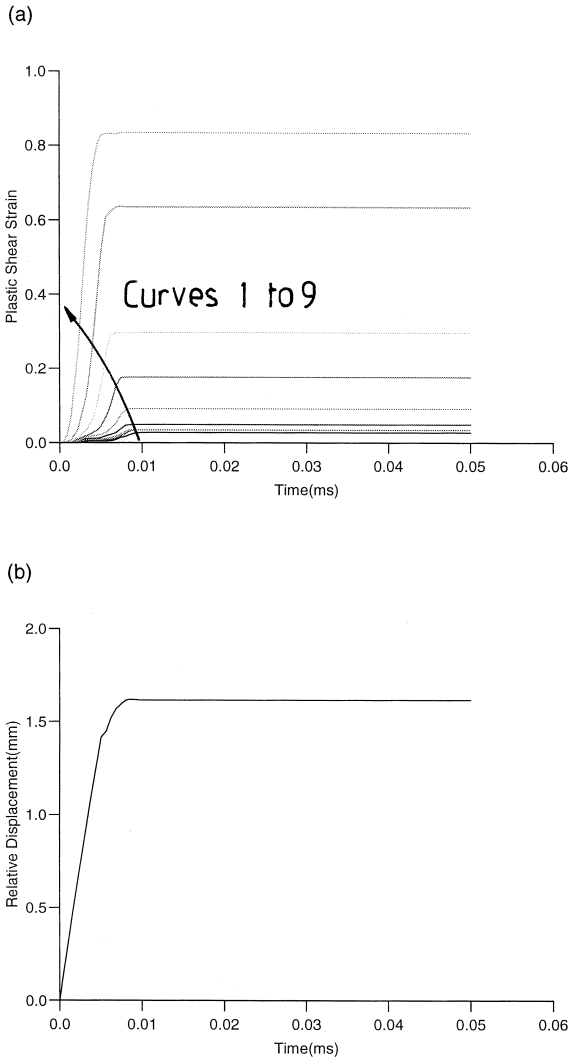

Fig. 10. (a) Plastic shear and equivalent strain histories at different locations along the shear hinge length in simulation H1, curves 1, 2, … … 9 correspond to elements 296, 306, … … 376 shown in Fig. 3; (b) relative displacement across the shear hinge length, e.

4. Discussion

The actual dynamic transverse loads, which act on structures, are more complicated than the idealized case considered in the previous sections. Two typical dynamic loadings in impact engineering are mass impact loadings and explosive pressure loads, which may produce a transverse shear localization at either the periphery of an impacted area or at any hard-points, such as supports. The characteristic velocities and loading times in these cases are determined from the initial impact velocities and input energies. Within the early stage of the response, a compressive wave propagates from the top surface to

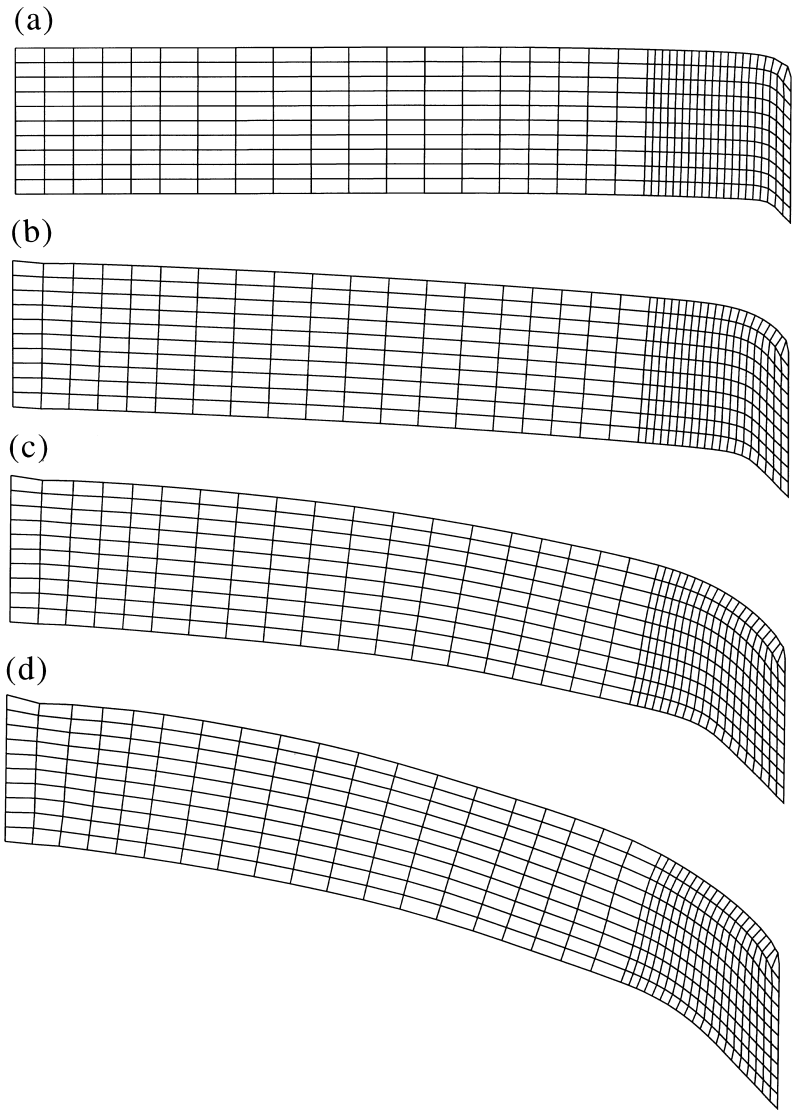

Fig. 11. Deformation patterns of a beam with an imposed velocity of $V = 300$ m/s, (a) $W = 1.5$ mm and $T = 5$ μs (H1); (b) $W = 3.0$ mm and $T = 10$ μs (H9); (c) $W = 6.0$ mm and $T = 20$ μs (H10); (d) $W = 9.0$ mm and $T = 30$ μs (H13).

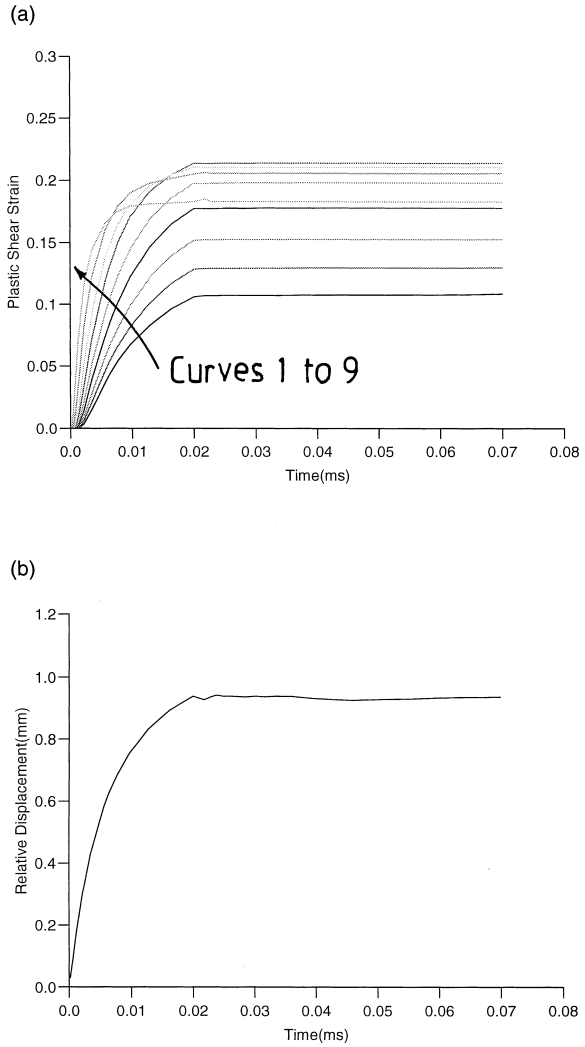

Fig. 12. (a) Shear strain histories with strain rate effects ($W = 3.0$ mm and $T = 20$ μs in H8), curves 1, 2, ... 9 correspond to elements 296, 306, ... 376 shown in Fig. 3; (b) relative displacement across the length of a shear hinge when retaining strain rate effects (H8).

the bottom surface of a structural element and produces a transverse disturbance. When the impact velocity is sufficiently high, considerable indentation and local failure may occur during this stage. The interactions between the indentation/failure and shear propagation must be considered for a realistic prediction of the behaviour. Several practical models have been developed by Awerbuch and Bodner (1974) for this purpose and the perforated profiles of the plate cross-section in Figs. 3 and 5 of Awerbuch and Bodner (1974) are comparable with the deformation shape near the loading boundary shown in Fig. 4(c) of the current simulation for a beam.

For intensive dynamic loading, the material properties may change significantly, which can only be simulated by a more complicated material model. Even within the dynamic plastic response range, strain

rate and temperature effects are important for medium to high speed loadings. An adiabatic shear band may be initiated during the shear propagation period due to thermal softening of the material, which may prevent further extension of the conventional shear zone. Instead, a more severe shear localization with a band width around 10–100 μm may be formed and material fractures initiate within this band. The band width is determined mainly by the material properties and is independent of the size of a conventional shear hinge. This feature is similar to a shear hinge which is determined mainly by the structural element properties, such as Q_0 and M_0 for a beam, and is independent of the size of the structural element, e.g. the beam length.

In many cases, the temperature effect becomes important only after considerable plastic work has been consumed by a structure, but, strain rate effects are always important for rate sensitive materials. Therefore, the influence of material strain rate sensitivity should be retained in analyses of transverse shear propagation. Numerical simulations for the same beam without (H6) and with (H8) strain rate effects were conducted. The Cowper–Symonds relationship given by Eq. (23) with $D = 6500$ (1/s) and $p = 4.0$ was used to examine the influence of strain rate effects for 6061-T6 aluminum alloy. It is found that the magnitude of the transverse shear strain without considering strain rate effect (H6) is larger than that when strain rate effects are considered (H8). Actually, the maximum shear strain is 0.38 for simulation H6 when the strain rate effect is neglected, which is nearly double the value obtained for H8 when the influence of material strain rate sensitivity is retained. These results imply that the stress state, or the dynamic yield stress, is another important factor which influences the magnitude of the maximum shear strain in addition to the impact velocity.

The shear strain histories and the relative displacement across the length of a shear hinge in a strain rate sensitive beam are shown in Fig. 12(a) and (b). The maximum shear strain from Eq. (26) and Fig. 12(b) is 0.22, which is comparable with $\gamma_{\max} = 0.218$ from the ABAQUS results in Fig. 12(a). Thus, Eq. (26) appears to remain valid for strain rate sensitive materials.

Finally, it should be noted that the broad conclusions of this study for a beam might be applicable to plates and cylindrical shells when subjected to large dynamic transverse loads due to the similarities inherent in all transversely loaded structural elements.

5. Conclusions

A transverse shear hinge is an important concept in dynamic rigid, perfectly plastic analyses. The geometrical size of a transverse shear hinge is obtained for beams, circular plates and cylindrical shells using a quasi-static method of analysis. With the aid of dimensional analysis, the formation of a transverse shear hinge in a beam is examined using finite-element simulations. It is found that quasi-static predictions and the concept of a transverse shear hinge are valid when the impact velocity is the same order as the plastic shear wave speed. When the impact velocity is much smaller than the plastic shear speed, bending dominates the response. On the other hand, if the impact velocity is larger than the plastic shear speed, then in-plane plastic shear wave propagation is important. Although the finite-element simulation is based on an idealised beam problem, it reflects the general features of a transverse shear hinge.

Acknowledgements

The first author would like to acknowledge the financial support from the Impact Research Centre, The University of Liverpool. Other grants from the Christine King Memorial Trust, Henry Lester Trust,

John Lennon Memorial Scholarship, the Great Britain-China Educational Trust and an ORS Award are also gratefully acknowledged.

References

ABAQUS, 1996a. Theory and User's Manual/Standard, Version 5.5.

ABAQUS, 1996b. Example Problems Manual/Standard, Vol. II, Version 5.5, Section 5.2.4-1.

Awerbuch, J., Bodner, S.R., 1974. Experimental investigation of normal perforation of projectiles in metallic plates. Int. J. of Solids and Structures 10, 685–699.

Gomes de Oliveira, J., Jones, N., 1978. Some remarks on the influence of transverse shear on the plastic yielding of structures. Int. J. of Mech. Sci. 20, 759–765.

Jones, N., 1976. Plastic failure of ductile beams loaded dynamically. Trans. ASME, J. Engng Ind. 98, 131–136.

Jones, N., 1985. Bounds on the dynamic plastic behaviour of structures including transverse shear effects. Int. J. of Impact Engineering 3, 273–291.

Jones, N., 1989a. Structural Impact. Cambridge University Press Paperback ed. (1997).

Jones, N., 1989b. Recent studies on the dynamic behavior of structures. Appl. Mech. Rev. 42, 95–115.

Jones, N., 1989c. On the dynamic inelastic failure of beams. In: Wierzbicki, T., Jones, N. (Eds.), Structural Failure. Wiley, New York, pp. 133–159.

Jones, N., Shen, W.Q., 1993. Criteria for the inelastic rupture of ductile metal beams subjected to large dynamic loads. In: Jones, N., Wierzbicki, T. (Eds.), Structural Crashworthiness and Failure. Elsevier, London, pp. 95–130.

Jones, N., Kim, S.B., Li, Q.M., 1997. Response and failure analysis of ductile circular plates struck by a mass. Trans. ASME J. of Pressure Vessel Tech. 119, 332–342.

Li, Q.M., Jones, N., 1994. Blast loading of fully clamped circular plates with transverse shear effects. Int. J. of Solids and Structures 31, 1861–1876.

Li, Q.M., Jones, N., 1995a. Blast loading of fully clamped beams with transverse shear effects. Mechanics of Structures and Machines 23, 59–86.

Li, Q.M., Jones, N., 1995b. Blast loading of a 'short' cylindrical shell with transverse shear effects. Int. J. of Impact Engineering 16, 331–353.

Li, Q.M., 2000. Continuity conditions at bending and shearing interfaces of rigid, perfectly plastic structural elements. Int. J. of Solids and Structures 37, 3651–3665.

Li, Q.M., Jones, N., 1999. Shear and adiabatic shear failures in an impulsively loaded fully clamped beam. Int. J. of Impact Engineering 22, 589–607.

Menkes, S.B., Opat, H.J., 1973. Broken beams. Exp. Mech. 13, 480–486.

Reid, S.R., Gui, X.G., 1987. On the elastic-plastic deformation of cantilever beams subjected to tip impact. Int. J. of Impact Engineering 6, 109–127.

Symonds, P.S., 1968. Plastic shear deformation in dynamic load problems. In: Heyman, J., Leckie, F.A. (Eds.), Engineering Plasticity. Cambridge University Press, Cambridge, pp. 647–664.

Wang, L.L., Jones, N., 1996. An analysis of the shear failure of rigid-linear hardening beams under impulsive loading. Acta Mechanica Sinica 12 (4), 338–348 (English Series).

Wen, H.M., Reddy, T.Y., Reid, S.R., 1995a. Deformation and failure of clamped beams under low speed impact loading. Int. J. of Impact Engineering 16, 435–454.

Wen, H.M., Yu, T.X., Reddy, T.Y., 1995b. Failure maps of clamped beams under impulsive loading. Mech. Struct. Machine 23, 453–472.

Wen, H.M., Yu, T.X., Reddy, T.Y., 1995c. A note on clamped circular plates under impulsive loading. Mech. Struct. Machine 23, 331–342.

Wen, H.M., Jones, N., 1996. Low-velocity perforation of punch-impact-loaded metal plates. Trans. ASME J. of Pressure Vessel Tech. 118, 181–187.

Yu, J.L., Jones, N., 1989. Numerical simulation of a clamped beam under impact loading. Computers and Structures 32, 281–293.

Yu, J.L., Jones, N., 1997. Numerical simulation of impact loaded steel beams and the failure criteria. Int. J. of Solids Structures 34, 3977–4004.

Yu, T.X., Yang, J.L., Reid, S.R., 1997. Interaction between reflected elastic flexural waves and a plastic 'hinge' in the dynamic response of pulse loaded beams. Int. J. of Impact Engineering 19, 457–475.

Zener, C., 1948. The micro-mechanism of fracture. In: Sachs, G. (Ed.), Fracturing of Metals. American Society for Metals, Cleveland, Ohio, pp. 3–31.